

A molnupiravir-associated mutational signature in global SARS-CoV-2 genomes

Theo Sanderson¹
Ryan Hisner²
I'ah Donovan-Banfield^{3,4}
Hassan Hartman⁵
Alessandra Løchen⁵
Thomas P. Peacock^{6,7}
Christopher Ruis^{8,9,10}

¹ Francis Crick Institute, London, UK

² Department of Bioinformatics, University of Cape Town, Cape Town, South Africa

³ Department of Infection Biology and Microbiomes, Institute of Infection, Veterinary and Ecological Sciences, University of Liverpool, Liverpool, UK

⁴ NIHR Health Protection Research Unit in Emerging and Zoonotic Infections, Liverpool, UK

⁵ UK Health Security Agency, London, UK

⁶ Department of Infectious Disease, Imperial College London, London, UK

⁷ The Pirbright Institute, Pirbright, UK

⁸ Molecular Immunity Unit, University of Cambridge Department of Medicine, MRC-Laboratory of Molecular Biology, Cambridge, UK

⁹ Department of Veterinary Medicine, University of Cambridge, Cambridge, UK

¹⁰ Cambridge Centre for AI in Medicine, University of Cambridge, Cambridge, UK

A molnupiravir-associated mutational signature in global SARS-CoV-2 genomes

Theo Sanderson^{1,✉}, Ryan Hisner², I'ah Donovan-Banfield^{3,4}, Hassan Hartman⁵, Alessandra Løchen⁵, Thomas P. Peacock^{6,7}, and Christopher Ruis^{8,9,10,✉}

¹Francis Crick Institute, London, UK; ²Department of Bioinformatics, University of Cape Town, Cape Town, South Africa; ³Department of Infection Biology and Microbiomes, Institute of Infection, Veterinary and Ecological Sciences, University of Liverpool, Liverpool, UK; ⁴NIHR Health Protection Research Unit in Emerging and Zoonotic Infections, Liverpool, UK; ⁵UK Health Security Agency, London, UK; ⁶Department of Infectious Disease, Imperial College London, London, UK; ⁷The Pirbright Institute, Pirbright, UK; ⁸Molecular Immunity Unit, University of Cambridge Department of Medicine, MRC-Laboratory of Molecular Biology, Cambridge, UK; ⁹Department of Veterinary Medicine, University of Cambridge, Cambridge, UK; ¹⁰Cambridge Centre for AI in Medicine, University of Cambridge, Cambridge, UK

Molnupiravir, an antiviral medication that has been widely used against SARS-CoV-2, acts by inducing mutations in the virus genome during replication. Most random mutations are likely to be deleterious to the virus, and many will be lethal, and so molnupiravir-induced elevated mutation rates reduce viral load^{2,3}. However, if some patients treated with molnupiravir do not fully clear SARS-CoV-2 infections, there could be the potential for onward transmission of molnupiravir-mutated viruses. Here we show that SARS-CoV-2 sequencing databases contain extensive evidence of molnupiravir mutagenesis. Using a systematic approach, we find that a specific class of long phylogenetic branches, distinguished by a high proportion of G-to-A and C-to-T mutations, appear almost exclusively in sequences from 2022, after the introduction of molnupiravir treatment, and in countries and age-groups with widespread usage of the drug. We identify a mutational spectrum, with preferred nucleotide contexts, from viruses in patients known to have been treated with molnupiravir and show that its signature matches that seen in these long branches, in some cases with onwards transmission of molnupiravir-derived lineages. Finally, we analyse treatment records to confirm a direct association between these high G-to-A branches and the use of molnupiravir.

Correspondence: theo.sanderson@crick.ac.uk cr628@cam.ac.uk

Molnupiravir is an antiviral drug, licensed in some countries for the treatment of COVID-19. In the body, molnupiravir is ultimately converted into a nucleotide-analog, molnupiravir triphosphate (MTP)¹. MTP is incorporated into RNA during strand synthesis by viral RNA-dependent RNA polymerases, where it can result in errors of sequence fidelity during viral genome replication. These errors result in many viral progeny that are non-viable, and so reduce the virus's effective rate of growth – molnupiravir was shown to reduce viral replication during 24 hours by 880-fold in vitro, and to reduce viral load both in animal models² and in patients sampled on the final day of treatment³. Molnupiravir initially

showed some limited efficacy as a treatment for COVID-19^{4,5}, but subsequently the much larger PANORAMIC trial found that treatment did not reduce hospitalisation or death rates in a group of largely vaccinated high-risk individuals³. As one of the first orally bioavailable antivirals on the market, molnupiravir was widely adopted in many countries. However, recent trial results and the approval of more efficacious antivirals have since led to several countries recommending against its use^{6–8}, while longstanding concerns have been raised about potential mutagenic activity in host cells⁹.

MTP appears to be incorporated into nascent RNA primarily by acting as an analogue of cytosine (C), pairing opposite guanine (G) bases (Fig. 1A). However, once incorporated, the molnupiravir (M)-base can transition into an alternative tautomeric form which resembles uracil (U) instead. This means that in the next round of strand synthesis, giving the positive-sense SARS-CoV-2 genome, the tautomeric M base pairs with adenine (A), resulting in a G-to-A mutation (Fig. 1B). These G-to-A mutations arise from incorporation of molnupiravir into the negative-sense genome. Incorporation of MTP can also occur during the synthesis of the positive-sense genome: in this scenario, an initial positive-sense C correctly pairs with a G during negative-sense synthesis, but this G then pairs with an M base during positive-sense synthesis. In the next round of replication this M can then pair with A, which will result in a U in the final positive sense genome, with the overall process producing a C-to-U mutation (Fig. 1C). The free nucleotide MTP is less prone to tautomerisation to the oxime form than when incorporated into RNA, and so this directionality of mutations is the most likely¹⁰. However it is also possible for some MTP to bind, in place of U, to A bases and undergo the above processes in reverse, causing A-to-G and U-to-C mutations (Fig. 1C).

It has been proposed that many major SARS-CoV-2 variants emerged from long-term chronic infections. This model explains several peculiarities of variants such as a general lack of genetic intermediates, rooting with much older sequences, long phylogenetic branch lengths, and the level of convergent evolution with known chronic infections^{11–14}. During the approval process for molnupiravir, concerns were raised about its potential to increase the rate of evolution of variants of

¹MTP is also known as β-D-N⁴-hydroxycytidine triphosphate (NHC-TP).

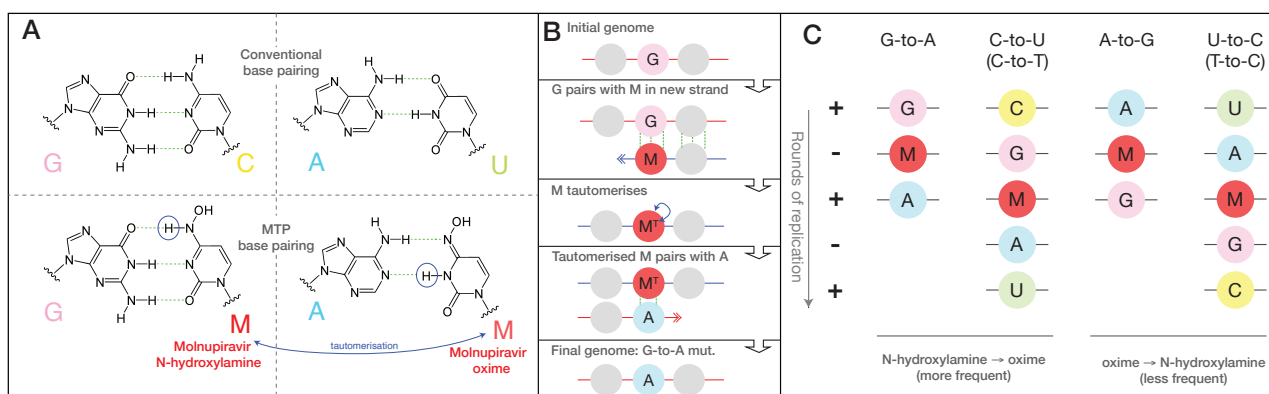


Figure 1. Molnupiravir induces mutations by acting as a nucleotide analogue with multiple tautomeric forms which pair preferentially with different nucleotides. (A) Molnupiravir triphosphate can assume multiple tautomeric forms which resemble different nucleotides. The N-hydroxylamine form resembles cytosine (C), and like cytosine can pair with guanine (G) while the oxime form more closely resembles uracil (U), and thus can pair with adenine (A). (Figure adapted in part from Malone et al.¹) (B) In the most common scenario, molnupiravir (M) is incorporated in the N-hydroxylamine form opposite a G nucleotide. It can then tautomerise into the oxime form, which can then pair to an A in subsequent replication, creating a G-to-A mutation. (C) Molnupiravir can result in four different mutation types. In the first column a G-to-A mutation is created by M incorporation opposite a positive-sense G, which can then pair with an A in the next positive-sense synthesis. In the second column, the positive-sense genome contains a C, which results in a G in the negative-sense genome. This G can then undergo the same G-to-A mutation, creating a negative-sense A which finally results in a U in the positive sense genome, meaning the entire process results in a C-to-U mutation. Although the biases of tautomeric forms for the free and incorporated MTP nucleotides appear to favour this directionality of mutations, with M incorporated in the N-hydroxylamine form and then transitioning to the oxime form, the reverse can also occur: this results in A-to-G and U-to-C mutations.

concern¹⁵. In response, it was noted that no infectious virus had been isolated at or beyond day 5 of molnupiravir treatment, and that mutations recovered following treatment were random with no evidence of selection-based bias¹⁶.

During analysis of divergent SARS-CoV-2 sequences, signs of molnupiravir-driven mutagenesis have been noted¹⁷, including indications of possible transmission. We therefore aimed to characterise the mutational profile of molnupiravir and examine the extent to which this signature appeared in global sequencing databases.

Emergence of a new mutational signature

To establish the mutational profile induced by molnupiravir, we analysed published longitudinal genomic time series that included both untreated patients and patients treated with molnupiravir^{18,20}, and compared against a typical SARS-CoV-2 mutational spectrum¹⁹. In agreement with previous findings, we found that molnupiravir treatment led to an 8-fold increase (CI: 2.9-16) in the rate of mutations and that this increase was highly specific to transition mutations (Fig. 2A), especially to G-to-A and C-to-T mutations (hereon we use 'T' rather than 'U', as in sequences). While C-to-T mutations are relatively common overall in SARS-CoV-2 evolution^{19,21,22}, G-to-A mutations occur much less frequently; therefore an elevated G-to-A proportion was especially predictive of molnupiravir treatment (Fig. 2B).

We looked for evidence of such a signal in global sequencing databases by analysing a mutation-annotated tree, derived from McBroome et al.²³, containing >15 million SARS-CoV-2 sequences from GISAID²⁴ and the INSDC databases²⁵. For each branch of the tree we counted the number of each substitution class (A-to-T, A-to-G, etc.). Filtering this tree to branches involving at least 20 substitutions, and plotting the proportion of

substitution types revealed a region of this space with higher G-to-A and almost exclusively transition substitutions, that only contained branches sampled since 2022 (Fig. 2C), suggesting some change (either biological or technical) had resulted in a new mutational pressure, with mutational classes consistent with those seen in patients known to be treated with molnupiravir.

We created a criterion for branches of interest, which we refer to as "high G-to-A" branches: we selected branches involving at least 10 substitutions, of which more than 25% were G-to-A, more than 20% were C-to-T and more than 90% were transitions. Simulations predicted that this criterion would have a sensitivity of 63% and a specificity of 98.6% for branches involving 13 substitutions (see methods). Branches satisfying the high G-to-A conditions were almost all sampled after the roll-out of molnupiravir in late 2021 and early 2022 (Fig. 2D, Extended Data 1). The branches were predominantly sampled from a small number of countries, which could not be explained by differences in sequencing efforts (Fig. 2E-F, Extended Data 2). Many countries which exhibited a high proportion of high G-to-A branches use molnupiravir: >380,000 prescriptions had occurred in Australia by the end of 2022²⁶, >30,000 in the UK in the same period^{3,27}, >240,000 in the US within the early months of 2022²⁸, and >600,000 in Japan by Oct 2022²⁹. Countries with high levels of total sequencing but a low number of G-to-A branches (Canada, France, Fig. 2E-F) have not authorised the prescription of molnupiravir^{30,31}. Age metadata from the US showed a significant bias towards samples from patients of older ages for these high G-to-A branches, compared to control branches with similar numbers of mutations but without filtering on substitution-type (Fig. 2G). Where age data was available in Australia it also suggested high G-to-A branches primarily occur in

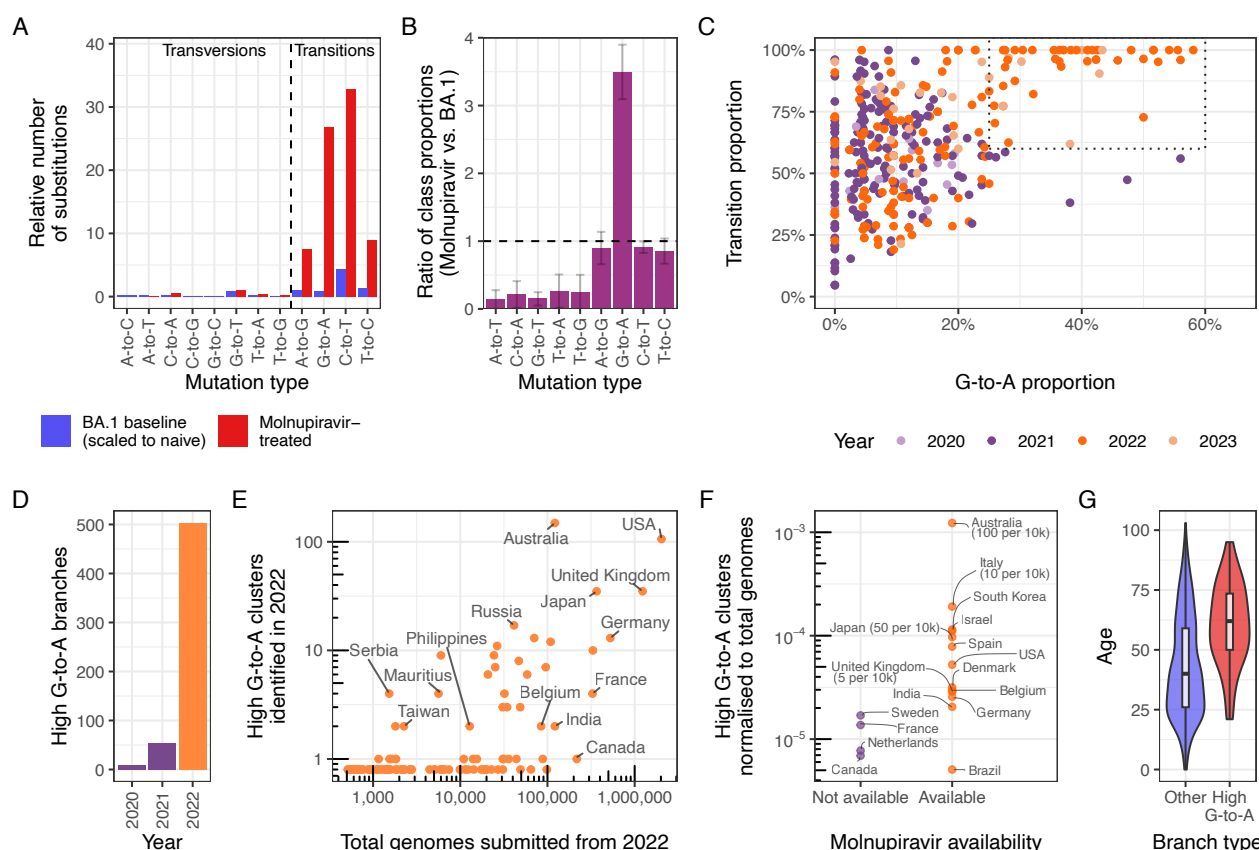


Figure 2. A molnupiravir-associated mutational signature with high G-to-A and high transition ratio emerged in 2022 in some countries in global sequencing databases

(A) A comparison the relative rate of different classes of mutations in typical BA.1 mutations vs. those with molnupiravir treatment (molnupiravir data from Alteri et al.¹⁸; naive data from Ruis et al.¹⁹, scaled to total mutations in naive individuals from Alteri et al., see Methods) confirms an elevated rate of transitions, and particularly C-to-T and G-to-A mutations. (B) Differences in the proportion of mutations due to different mutation classes in molnupiravir-treated individuals (Alteri et al.¹⁸) vs typical BA.1 mutations (Ruis et al.¹⁹) highlights elevated G-to-A proportion as especially indicative of molnupiravir. These are ratios of proportions and so the apparent reduction in transversions does not require an absolute decrease in the number of transversions, but can instead be caused by the increased number of transitions. Error bars represent 95% confidence intervals. (C) A scatter plot where each point is a branch with >20 mutations, positioned according to the proportion of these mutations that are G-to-A (x-axis) or transitions (y-axis) reveals a space with elevated G-to-A and transition rate that occurs only with the rollout of molnupiravir in 2022, as also shown in (D) for nodes with >10 mutations, G-to-A proportions >25%, C-to-T proportions >20%, and transition proportions >90%. (E) Plotting the number of high G-to-A nodes identified in 2022 against the number of total genomes for each country reveals considerable variation. (F) Countries confirmed to have made molnupiravir available have more high G-to-A nodes than countries which have not. Numbers in brackets represent number of courses of molnupiravir supplied, normalised to population. ($p=0.02$ for log-transformed two-sided t-test.) (G) Age distribution for US nodes, partitioned according to whether they satisfy the high G-to-A criterion ($p<1e-10$, two-sided t-test). Age metadata are missing for some samples, likely non-randomly. Where a node has many descendants of different ages, age is assigned by a basic heuristic, as described in the methods. Boxplot depicts minimum, maximum, and 25th, 50th and 75th percentiles.

an aged population. This is consistent with the prioritised use of molnupiravir to treat older individuals, who are at greater risk from severe infection, in these countries. In Australia, molnupiravir was pre-placed in aged-care facilities, and it was recommended that it be considered for all residents testing positive for COVID-19 aged 70 or older, with or without symptoms³².

Mutation contexts support molnupiravir link

To further probe the link between high G-to-A branches and molnupiravir, we used mutation spectrum analysis, which considers both the types of mutations and the genomic context in which the mutations occur (Extended Data 5). The spectrum we identified for branches selected by these criteria was, as expected, dominated by G-to-A and C-to-T transition mutations with smaller contributions from A-to-G and T-to-C transitions (Fig. 3A). We similarly calculated spectra both from patients

known to be treated with molnupiravir^{18,20} (Fig. 3B) and from general SARS-CoV-2 evolution¹⁹ (Fig. 3C).

There was a strong match between the spectrum of known-molnupiravir sequences and that of high G-to-A branches, both in terms of mutation classes and the context preferences within each mutation class (Fig. 3, Extended Data 6A). For C-to-T and G-to-A mutations, a comparison of context preferences gave cosine similarities of 0.988 and 0.965 respectively (Fig. 3D). Similar results were seen for a spectrum calculated from a separate second dataset from a clinical trial of molnupiravir (Extended Data 6B)²⁰. The contextual patterns seen in long branches did not correlate with typical SARS-CoV-2 mutational processes (Extended Data 6C). In high G-to-A branches, G-to-A mutations occurred most commonly in TGT and TGC contexts, which could represent a preference for molnupiravir binding adjacent to particular surrounding nucleotides, a preference of the viral

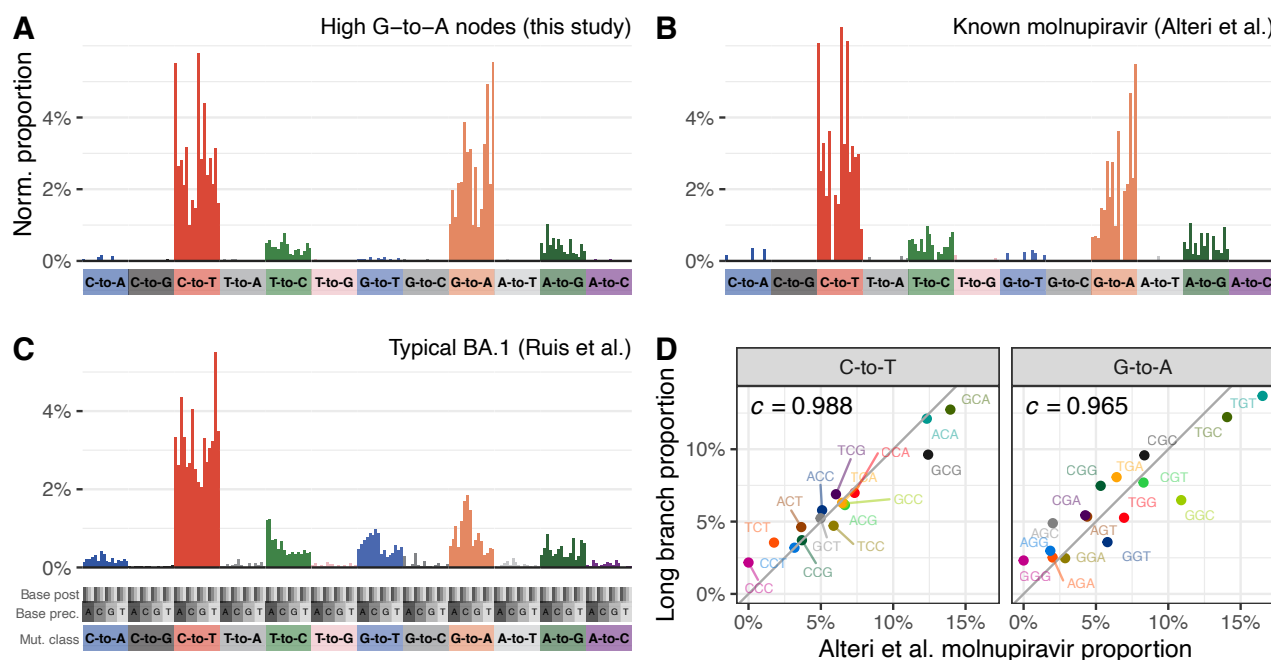


Figure 3. Mutation spectrum analysis supports high G-to-A branches being driven by molnupiravir

(A,B,C) Single-base substitution mutation spectra for high G-to-A branches (A), known molnupiravir-treated individuals (B) and typical BA.1 spectra (C). Each individual bar represents a particular type of mutation in a particular trinucleotide context (Extended Data 5). Bars are grouped and coloured according to the class of mutation. Within each coloured group, bars are grouped into 4 groups according to the nucleotide preceding the mutated residue, and then each of these groups contains 4 bars according to the nucleotide following the mutated residue. Number of mutations have been normalised so that the entire spectrum sums to 1. (D) High correlations between spectra from Alteri et al. from patients known to have been treated with molnupiravir, and the spectra from high G-to-A branches identified in this study. Each point represents the normalised proportion of a particular trinucleotide context. Points are coloured such that a context for C-to-T mutations has the same colour as its reverse complement in G-to-A. The values denoted by c are cosine similarity scores.

RdRp to incorporate molnupiravir adjacent to specific nucleotides, or a context-specific effect of the viral proof-reading machinery. These correlations between spectra from high G-to-A branches and known molnupiravir-treated individuals strongly support a shared mutational driver, and therefore that the high G-to-A branches are driven by molnupiravir treatment.

Incorporation of molnupiravir during negative strand synthesis will result in G-to-A mutations in the virus sequence while incorporation during positive strand synthesis will manifest as C-to-T mutations in the virus sequence, after a second round of replication (Fig. 1C). Consistent with this, we observe a strong similarity between the mutational biases in equivalent surrounding contexts within C-to-T and G-to-A mutations when comparing reverse complement triplets, with for example a G-to-A mutation in the TGC context on one strand being equivalent to a C-to-T mutation in the GCA context on the other strand (cosine similarity: 0.955, Extended Data 6D).

Transmission clusters and mutation rates

Although a majority of the long branches identified have just a single descendant tip sequence in sequencing databases, in some cases we could see that branches had given rise to clusters with a significant number of descendant sequences. For example, a cluster in Australia in August 2022 involves 20 tip sequences, with dis-

tinct age metadata confirming they derive from multiple individuals (Fig. 4A). This cluster involves 25 substitutions in the main branch, of which all are transitions with 44% C-to-T and 36% G-to-A. Closely related outgroups date from July 2022, suggesting that these mutations emerged in a period of 1-2 months. At the typical rate of SARS-CoV-2 evolution, this number of mutations would take years to acquire in an unsampled population with typical dynamics³³. Overall in the dataset, we observe a systematic accelerated evolutionary rate in high G-to-A branches ($p < 0.001$), consistent with the action of a mutagenic drug.

There are many further examples of high G-to-A branches with multiple descendant sequences, including sequence clusters in the United Kingdom, Japan, USA, New Zealand, Slovakia, Denmark, South Korea and Vietnam (Fig. 4B, Supplement 1).

During the construction of the daily-updated mutation-annotated tree²³, samples highly divergent from the existing tree are excluded. This is a necessary step given the technical errors in some SARS-CoV-2 sequencing data, but means that highly divergent molnupiravir-induced sequences might be missed from this analysis. To search for excluded sequences with a molnupiravir-like pattern of mutations we processed a full sequence dataset with Nextclade and calculated the proportion of each of the mutation classes among the private mutations (see methods) each sequence carried. This

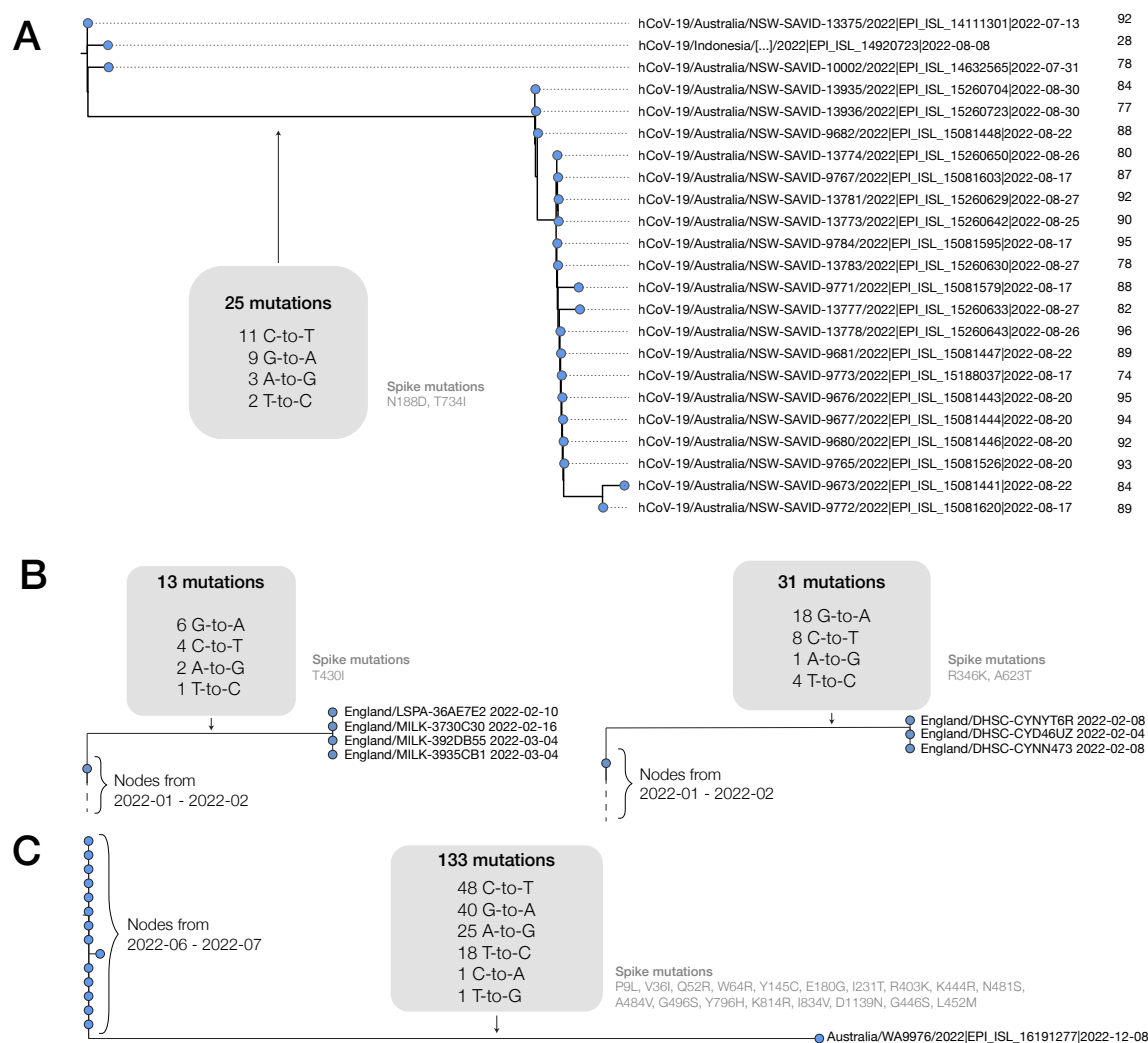


Figure 4. High G-to-A branches can be associated with transmission clusters and, separately, can involve more than 100 mutations

(A) A cluster of 20 individuals emerging from a high G-to-A mutation event. This cluster involves a saltation of 25 mutations occurring within a period of around a month, all of which are transition substitutions, with an elevated G-to-A rate. Sequences are annotated with age metadata suggestive of an outbreak in an aged-care facility. Phylogenetic placement within the cluster is affected by missing coverage in some regions. (B) Examples of further transmission clusters from the UK, left: four sequences from the UK from Feb-March 2022 with 13 shared mutations with the high G-to-A signature, right: a cluster of four sequences from the UK from Feb 2022 with 31 shared mutations with the high G-to-A signature. (C) A sequence from Australia with a high G-to-A signature and a total of 133 mutations relative to the closest outgroup sequence. Just 2 of the 133 mutations observed are transversions and transitions include numerous G-to-A events. (In the month after this sequence was deposited two additional related/descendant sequences – EPI_ISL_16315710, EPI_ISL_16639468 – were deposited, which may represent continued sampling from the same patient since they involve a substantial subset of shared mutations, but not full concordance, suggestive of complex intra-host evolution.)

analysis allowed the identification of further mutational events, including some involving up to 130 substitutions (Fig. 4C, Extended Data 3), with the same signature of elevated G-to-A mutation rates and almost exclusively transition substitutions. The cases we identified with these very high numbers of mutations predominantly involved single sequences, and could represent sequences resulting from chronically infected individuals who have been treated with multiple courses of molnupiravir. We verified that nucleotide contexts of the transition mutations observed within the sequence in Fig. 4C were much more likely under the molnupiravir spectrum than the typical BA.1 spectrum (Bayes factor $>10^{10}$).

Effects of molnupiravir-induced mutations

High G-to-A branches made up a considerable percentage of branches involving more than 10 substitutions in some countries (Fig. 5A), suggesting that molnupiravir drives a substantial proportion of large saltations. We found that high G-to-A branches had a different distribution of branch lengths from other types of branches. In typical SARS-CoV-2 evolution, the branch length distribution contains many more nodes with shorter branch lengths than with larger branch lengths, however for nodes satisfying the high G-to-A criterion this decline was much less pronounced, with long branch lengths still relatively common (Fig. 5B).

We also examined whether the mutations identified induced changes to amino acid sequence (non-synonymous mutations) or not (synonymous mutations). We found that for short branches in the tree,

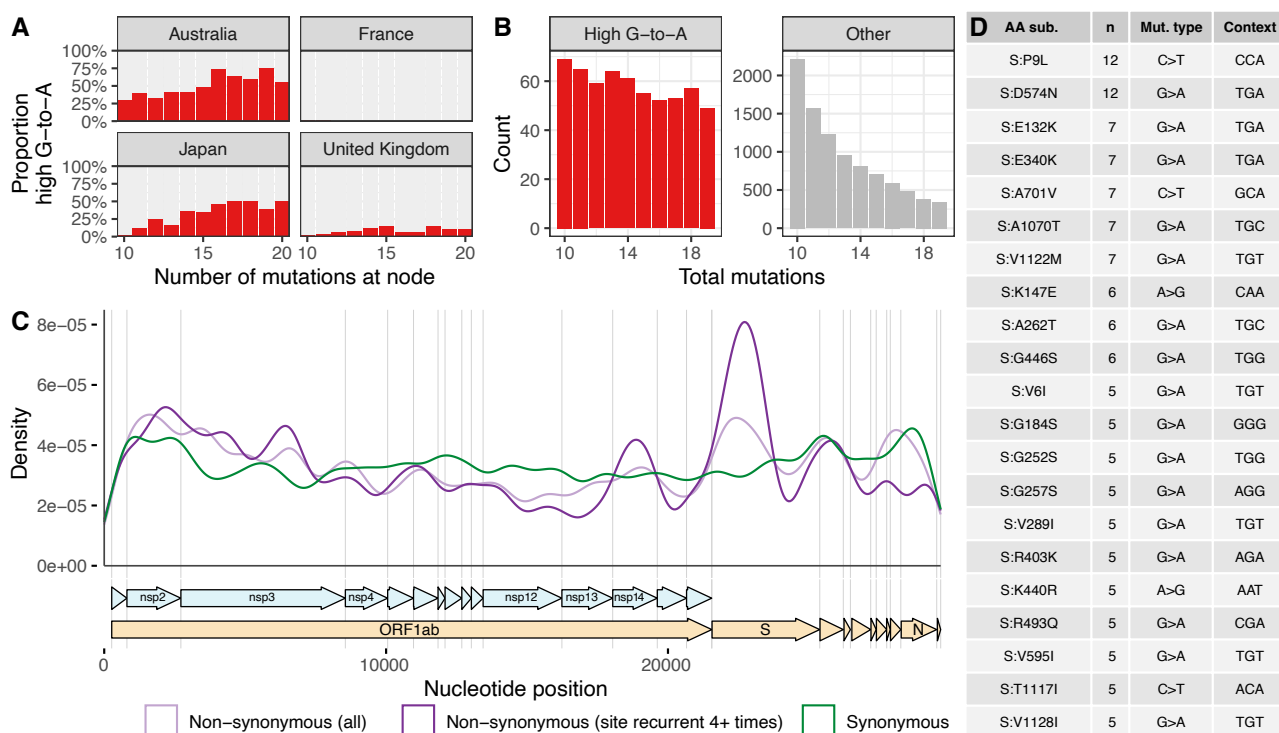


Figure 5. High G-to-A branches make up a considerable proportion of long branches in affected countries and include evidence of selection.

(A) Proportion of branches that are high G-to-A for a range of branch lengths in different countries. Data from collection dates in 2022 and 2023 (submission dates up to June 2023). (B) Branch length distributions for high G-to-A and other branches. (C) Genomic distribution of mutations in high G-to-A nodes, partitioned into 3 classes: synonymous mutations, non-synonymous mutations, and non-synonymous that occur 4 or more times. (D) Table of the most recurrent mutations in *spike* in high G-to-A branches. *n* shows the number of high G-to-A branches that exhibit the mutation. *Mutation type* shows the parental and final nucleotide at the nucleotide position driving the mutation, while *context* shows the trinucleotide context for the nucleotide mutated, transcribed assuming a NC₀45512.2 background.

65% (64.6%–64.7%) of mutations in the spike gene were non-synonymous. For long branches (≥ 10 mutations) that *lacked* the high G-to-A signature, the proportion of spike mutations that were non-synonymous was higher, at 77% (76.8%–77.55%). This increase may reflect, in part, positive selection during intra-host evolution in individuals with chronic infections. In contrast, for long branches with a (molnupiravir-associated) high G-to-A signature, the proportion of mutations in the spike protein that were non-synonymous was 63% (60.3%–65.1%), similar to that of short branches, and substantially lower than that of other long branches ($p < 0.001$).

Despite this overall indication of purifying selection, consistent with the actions of a mutagenic drug, there was also evidence for positive selection. Even in high G-to-A branches, there was a concentration of non-synonymous mutations in *spike*, especially among the most recurrent mutations (Fig. 5C). Many of the recurrent spike mutations, such as S:P9L, S:A701V, S:K147E, S:R493Q, and S:G252S, were also mutations that arise in variants of concern and/or chronic infections, including S:E340K which has been associated with sotrovimab resistance (Fig. 5D). There was good correspondence between the contexts in which these mutations occurred and the molnupiravir mutation spectrum. For example, the most common context for G-to-A class mutations among those listed in Fig. 5D is TGT, which has a high enrichment in the molnupiravir spectrum and a low enrichment in the normal BA.1 spectrum

(Extended Data 6C).

There was also a relative concentration of recurrent non-synonymous mutations in the exonuclease encoded by *nsp14*. This proofreading exonuclease functions to correct errors during genome replication, but typically has poor performance in recognising mismatches involving molnupiravir³⁴. Future work could examine whether there is a relationship between specific mutations in *nsp14* and tolerance to molnupiravir.

Confirmation from treatment records

To better test a direct relationship between high G-to-A branches and the use of molnupiravir, linkage analysis was performed for high G-to-A branches sampled in England with treatment data in the Blueteq database³⁵. This analysis found that 31% of clades descending from a high G-to-A branch involved an individual prescribed with molnupiravir (11 sequences in singleton clades; with sampling dates from day 7 to day 61 post treatment start date). The overall rate of molnupiravir prescription in sequenced individuals in England from 2022 is 0.043%.

Not all branches analysed were linked to a person known to have been prescribed molnupiravir. In some cases, these could represent false positives in our analysis. In addition, the Blueteq database does not contain prescription data for people treated as part of clinical trials (which make up around a third of total molnupiravir prescriptions in the UK) or patients who fell outside in-

terim clinical policy, and it is also possible that in some cases we have not sampled the index case treated with molnupiravir, but instead an individual downstream of a treated patient in a transmission chain.

Discussion

The observation that molnupiravir treatment has left a visible trace in global sequencing databases, including onwards transmission of molnupiravir-derived sequences, will be an important consideration for assessing the effects and evolutionary safety of this drug. Our results are consistent with recent observations in immunocompromised individuals³⁶.

New variants of SARS-CoV-2 are generated through acquisition of mutations that enhance properties including immune evasion and intrinsic transmissibility^{37,38}. The impact of molnupiravir treatment on the trajectory of variant generation and transmission is difficult to predict. A high proportion of induced mutations are likely to be deleterious or neutral, and it is important to consider a counterfactual to molnupiravir treatment which might involve higher viral load, potentially increasing the absolute number of diverse sequences^{39,40}. However molnupiravir increases per-sequence diversity in the surviving population, potentially with many mutations per genome, which might provide a broader substrate for selection to act on during intra-host evolution. Importantly, the divergence of the molnupiravir mutation spectrum from standard SARS-CoV-2 mutational forces might allow the virus to explore the fitness of distinctive parts of the possible genomic landscape to those it is already widely exploring in the general population. Molnupiravir-induced mutation could also potentially allow infections to persist for longer by creating a more varied target for the immune system: one concerning aspect of the PANORAMIC trial is that while molnupiravir-treated individuals had much lower viral load at day 5, they had slightly higher viral load than placebo-arm individuals at day 14³. It is notable that in some countries, a significant proportion of sequences with the longest branch lengths are attributable to molnupiravir. However, at the time of writing, the largest clusters satisfying our criteria consist of ~20 sequenced individuals.

Considerations of mechanism of action are important in the design and assessment of antiviral drugs. Molnupiravir's mode of action is often described using the term "error catastrophe" – the concept that there is an upper limit on the mutation rate of a virus beyond which it is unable to maintain self-identity⁴¹, but this model has been criticised on its own terms⁴² and is particularly problematic in the case of short-term antiviral treatment as it assumes an infinite time horizon. The "lethal mutagenesis" model is much more useful in this context⁴³. Not all nucleoside analog drugs function primarily through mutagenesis. Many act through chain-termination^{44,45}, and therefore would not be expected to cause the effects seen here for molnupiravir.

Our study illustrates the far-reaching potential of the extensive genomic dataset created by the community of researchers tracking SARS-CoV-2 evolution. The combination of all available global sequences increased the power of our analyses, while comparisons between countries with different treatment regimes were highly informative. We recommend that public health authorities perform continued investigations into the effects of molnupiravir in viral sequences, and the transmissibility of molnupiravir-derived lineages. These data will be useful for ongoing assessments of the risks and benefits of this treatment, and may guide the future development of mutagenic agents as antivirals, particularly for viruses with high mutational tolerances such as coronaviruses.

Bibliography

- Malone, B. & Campbell, E. A. Molnupiravir: coding for catastrophe. *Nat Struct Mol Biol* **28**, 706–708 (2021).
- Rosenke, K. *et al.* Orally delivered MK-4482 inhibits SARS-CoV-2 replication in the syrian hamster model. *Nat. Commun.* **12** (2021).
- Butler, J. Molnupiravir plus usual care versus usual care alone as early treatment for adults with COVID-19 at increased risk of adverse outcomes (PANORAMIC): an open-label, platform-adaptive randomised controlled trial. *Lancet* (2022).
- Jayk Bernal, A. *et al.* Molnupiravir for oral treatment of covid-19 in nonhospitalized patients. *N. Engl. J. Med.* **386**, 509–520 (2022).
- Extance, A. Covid-19: What is the evidence for the antiviral molnupiravir? *BMJ* **377**, o926 (2022).
- NICE recommends 3 treatments for COVID-19 in draft guidance. URL <https://www.nice.org.uk/news/article/nice-recommends-3-treatments-for-covid-19-in-draft-guidance>.
- NC19CET. Taskforce updates molnupiravir guidance following PANORAMIC trial results. <https://clinicalevidence.net.au/news/taskforce-updates-molnupiravir-guidance-following-panoramic-trial-results/> (2022). Accessed: 2023-1-6.
- Covid-19 antivirals: The role of molnupiravir in new zealand's funded treatments portfolio (2023). URL <https://pharmac.govt.nz/news-and-resources/consultations-and-decisions/consultation-2023-04-04-molnupiravir/?keyword=molnupiravir&type=all&page=1>.
- Waters, M. D., Warren, S., Hughes, C., Lewis, P. & Zhang, F. Human genetic risk of treatment with antiviral nucleoside analog drugs that induce lethal mutagenesis: the special case of molnupiravir. *Environmental and Molecular Mutagenesis* **63**, 37–63 (2022). URL <https://doi.org/10.1002/em.22471>.
- Gordon, C. J., Tchesnokov, E. P., Schinazi, R. F. & Götze, M. Molnupiravir promotes SARS-CoV-2 mutagenesis via the RNA template. *J. Biol. Chem.* **297** (2021).
- Rambaut, A. *et al.* Preliminary genomic characterisation of an emergent sars-cov-2 lineage in the uk defined by a novel set of spike mutations (2020). URL <https://virological.org/t/preliminary-genomic-characterisation-of-an-emergent-sars-cov-2-lineage-in-the-uk-defined-by-a-novel-set-of-spike-mutations/563>.
- Viana, R. *et al.* Rapid epidemic expansion of the SARS-CoV-2 Omicron variant in southern Africa. *Nature* **603**, 679–686 (2022).
- Hill, V. *et al.* The origins and molecular evolution of SARS-CoV-2 lineage B.1.1.7 in the UK. *Virus Evol* **8**, veac080 (2022).
- Harari, S. *et al.* Drivers of adaptive evolution during chronic SARS-CoV-2 infections. *Nat Med* **28**, 1501–1508 (2022).
- Nelson, C. W. & Otto, S. P. Mutagenic antivirals: the evolutionary risk of low doses. *Virological*. <https://virological.org/t/mutagenic-antivirals-the-evolutionary-risk-of-low-doses/768> [Google Scholar] (2021).
- Presentations to AMDAC Meeting. Antimicrobial drugs advisory committee meeting (AMDAC). <https://www.youtube.com/watch?v=FR9FNSJT64M> (2021). URL <https://www.fda.gov/media/155935/download>. Virtual Meeting, November 30, 2021.
- Hisner, R. RE: Potential BA.2.3 sublineage with many mutations (singleton, Indonesia). <https://github.com/cov-lineages/pango-designation/issues/1080#issuecomment-1250412876> (2022).
- Alteri C *et al.* A proof-of-concept study on the genomic evolution of sars-cov-2 in molnupiravir-treated, paxlovid-treated and drug-naïve patients. *Commun Biol* **5**, 1376 (2022).
- Ruis, C. *et al.* A lung-specific mutational signature enables inference of viral and bacterial respiratory niche. *Microbial Genomics* **9** (2023).
- Donovan-Banfield, I. *et al.* Characterisation of SARS-CoV-2 genomic variation in response to molnupiravir treatment in the AGILE Phase IIa clinical trial. *Nat Commun* **13**, 7284 (2022).
- Bloom, J. D., Beichman, A. C., Neher, R. A. & Harris, K. Evolution of the SARS-CoV-2 Mutational Spectrum. *Molecular Biology and Evolution* **40** (2023).

22. Tonkin-Hill, G. *et al.* Patterns of within-host genetic diversity in SARS-CoV-2 (2021).
23. McBroom, J. *et al.* A Daily-Updated database and tools for comprehensive SARS-CoV-2 Mutation-Annotated trees. *Mol. Biol. Evol.* **38**, 5819–5824 (2021).
24. Elbe, S. & Buckland-Merrett, G. Data, disease and diplomacy: GISAID's innovative contribution to global health. *Glob Chall* **1**, 33–46 (2017).
25. Cochrane, G., Karsch-Mizrachi, I., Nakamura, Y. & on behalf of the International Nucleotide Sequence Database Collaboration. The international nucleotide sequence database collaboration (2011).
26. <https://www.health.gov.au/resources/webinars/covid-19-response-update-for-primary-care-15-december-2022?language=en> (2022).
27. COVID Therapeutics Weekly Publication (week ending 1st January 2023). <https://www.england.nhs.uk/statistics/statistical-work-areas/covid-therapeutics-antivirals-and-neutralising-monoclonal-antibodies/> (2022).
28. Gold, J. A. W. *et al.* Dispensing of Oral Antiviral Drugs for Treatment of COVID-19 by Zip Code-Level Social Vulnerability - United States, December 23, 2021–May 21, 2022. *MMWR Morb Mortal Wkly Rep* **71**, 825–829 (2022).
29. Ministry of Health, L. & Welfare. Usage status of covid-19 therapeutics (government secured portion) (2023). URL https://www.mhlw.go.jp/stf/seisakunitsuite/bunya/0000121431_00324.html. Accessed: 2023-06-02; Original title: .
30. Drug and vaccine authorizations for COVID-19: List of authorized drugs, vaccines and expanded indications. <https://www.canada.ca/en/health-canada/services/drugs-health-products/covid19-industry/drugs-vaccines-treatments/authorization/list-drugs.html> (2022).
31. France cancels order for Merck's COVID-19 antiviral drug. <https://www.reuters.com/world/europe/france-cancels-order-mercks-covid-19-antiviral-drug-2021-12-22/> (2021).
32. Use of Lagevrio (molnupiravir) in residential aged care. URL <https://www.health.gov.au/sites/default/files/documents/2022/07/coronavirus-covid-19-use-of-lagevrio-molnupiravir-in-residential-aged-care.pdf>. Accessed: 2022-01-01.
33. Markov, P. V. *et al.* The evolution of SARS-CoV-2. *Nature Reviews Microbiology* **21**, 361–379 (2023). URL <https://doi.org/10.1038/s41579-023-00878-2>.
34. Sheahan, T. P. *et al.* An orally bioavailable broad-spectrum antiviral inhibits SARS-CoV-2 in human airway epithelial cell cultures and multiple coronaviruses in mice. *Science Translational Medicine* **12** (2020). URL <https://doi.org/10.1126/scitranslmed.abb5883>.
35. UK Health Security Agency. ESPAUR report 2021 to 2022: Annexe (2022). URL https://assets.publishing.service.gov.uk/government/uploads/system/uploads/attachment_data/file/1118730/ESPAUR-report-2021-2022-annexe.pdf. Accessed: 2023-06-26.
36. Fountain-Jones, N. M. *et al.* Antiviral treatments lead to the rapid accrual of hundreds of SARS-CoV-2 mutations in immunocompromised patients (2022).
37. Telenti, A., Hodcroft, E. & Robertson, D. The evolution and biology of SARS-CoV-2 variants. *Cold Spring Harbor Perspectives in Medicine* **12**, a041390 (2022).
38. Carabelli, A. M. *et al.* Sars-CoV-2 variant biology: immune escape, transmission and fitness. *Nature Reviews Microbiology* (2023).
39. Khoo, S. H. *et al.* Molnupiravir versus placebo in unvaccinated and vaccinated patients with early SARS-CoV-2 infection in the UK (AGILE CST-2): a randomised, placebo-controlled, double-blind, phase 2 trial. *Lancet Infect Dis* (2022).
40. Lobinska, G., Pilpel, Y. & Nowak, M. A. Evolutionary safety of lethal mutagenesis driven by antiviral treatment. *PLOS Biology* **21**, e3002214 (2023). URL <https://doi.org/10.1371/journal.pbio.3002214>.
41. Eigen, M. Selforganization of matter and the evolution of biological macromolecules. *Naturwissenschaften* **58**, 465–523 (1971).
42. Summers, J. & Litwin, S. Examining the theory of error catastrophe. *J. Virol.* **80**, 20–26 (2006).
43. Bull, J. J., n, R. & Wilke, C. O. Theory of lethal mutagenesis for viruses. *J Virol* **81**, 2930–2939 (2007).
44. Kovic, G. *et al.* Mechanism of SARS-CoV-2 polymerase stalling by remdesivir. *Nature Communications* **12** (2021). URL <https://doi.org/10.1038/s41467-020-20542-0>.
45. Clercq, E. D. & Neyts, J. Antiviral agents acting as DNA or RNA chain terminators. In *Antiviral Strategies*, 53–84 (Springer Berlin Heidelberg, 2009). URL https://doi.org/10.1007/978-3-540-79086-0_3.
46. Petit III, R. A., Hall, M. B., Tonkin-Hill, G., Zhu, J. & Read, T. D. fastq-dl: efficiently download FASTQ files from SRA or ENA repositories. URL <https://github.com/rpetit3/fastq-dl>.
47. Turakhia, Y. *et al.* Ultrafast Sample placement on Existing tRees (USHER) enables real-time phylogenetics for the SARS-CoV-2 pandemic. *Nat Genet* **53**, 809–816 (2021).
48. Sanderson, T. Taxonium, a web-based tool for exploring large phylogenetic trees. *Elife* **11** (2022).
49. McBroom, J., Turakhia, Y. & Corbett-Detig, R. BTE: a python module for pandemic-scale mutation-annotated phylogenetic trees. *Journal of Open Source Software* **7**, 4433 (2022). URL <https://doi.org/10.21105/joss.04433>.
50. Sanderson, T. Chronumetal: time tree estimation from very large phylogenies. *bioRxiv* (2021).
51. Hadfield, J. *et al.* Nextstrain: real-time tracking of pathogen evolution. *Bioinformatics* **34**, 4121–4123 (2018).
52. Aksamentov, I., Roemer, C., Hodcroft, E. & Neher, R. Nextclade: clade assignment, mutation calling and quality control for viral genomes. *Journal of Open Source Software* **6**, 3773 (2021).
53. Yu, G., Smith, D., Zhu, H., Guan, Y. & Lam, T. T.-Y. ggtree: an r package for visualization and annotation of phylogenetic trees with their covariates and other associated data. *Methods in Ecology and Evolution* **8**, 28–36 (2017).
54. Minh, B. Q. *et al.* Iq-TREE 2: New Models and Efficient Methods for Phylogenetic Inference in the Genomic Era. *Molecular Biology and Evolution* **37**, 1530–1534 (2020).
55. Sagulenko, P., Puller, V. & Neher, R. A. Treetime: Maximum-likelihood phylodynamic analysis. *Virus evolution* **4**, vex042 (2018). [Online; accessed 2023-01-13].
56. Rambaut, A. Figtree (2018). URL <http://tree.bio.ed.ac.uk/software/figtree/>.

Methods

Processing of pre-existing genomic data from molnupiravir treated individuals

We used three existing sources of genomic data in calculations of the mutational classes (and later the contextual mutational spectra) associated with known use of molnupiravir and with typical SARS-CoV-2 evolution in the absence of molnupiravir. We analysed a dataset from Alteri et al.¹⁸ which contained longitudinal data for both individuals treated with molnupiravir and untreated individuals. For this we downloaded FASTQ files from BioProject ERP142142 using `fastq-d1`⁴⁶. We mapped these reads to the Hu-1 reference genome using `minimap2` and then extracted the number of calls for each base at each position. We identified mutations compared to the day 0 sequence, counting variants where the site had ≥ 100 reads of which $\geq 5\%$ were variant to the day 0 consensus. As a secondary dataset we used data from the AGILE trial (Donovan-Banfield et al.²⁰, BioProject PRJNA854613). There was general agreement on the nature of molnupiravir mutations between Alteri et al. and the AGILE trial, with the exception of a high G-to-T mutation rate seen only in the AGILE trial. Previous evidence on molnupiravir's mutation classes, as well as the fact that a high G-to-T rate was seen even in untreated individuals in the AGILE data, led us to conclude that this G-to-T signal in the AGILE data represented a technical artifact.

We used the BA.1 mutational spectrum previously calculated by Ruis et al.¹⁹ as an exemplar of the mutation-classes and spectrum under typical SARS-CoV-2 evolution in the relevant time period. To compare mutation burden by mutation-class between molnupiravir-treated and untreated individuals we scaled the Ruis et al. dataset of typical BA.1 evolution to have the same number of total mutations as untreated individuals in the Alteri et al. dataset, and then plotted these against molnupiravir-treated individuals from the Alteri et al. dataset (Fig. 2A).

To identify which mutation-classes were diagnostic of the use of molnupiravir, we first calculated what proportion of mutations came from each mutation class, for both the Alteri et al. molnupiravir dataset and the Ruis et al. BA.1 dataset. We then calculated the ratio of these proportions between the molnupiravir and (naive) BA.1 datasets. To put confidence intervals on this ratio we performed bootstrap resampling from each set of mutations (with 100 bootstrap repeats). These data are presented in Fig. 2B.

Identification of high G-to-A sequences from UShER mutation-annotated tree

To identify sequences in global databases with a molnupiravir-like pattern of mutations, we analysed a regularly-updated mutation-annotated tree built by the UShER team⁴⁷ using almost all global data from INSDC and GISAID – a version of the McBroome et al. (2021)

tree²³. We extracted data using a script initially adapted from TaxoniumTools⁴⁸, and later modified to use the Big Tree Explorer (BTE)⁴⁹. The script added metadata from sequencing databases to each node, then passed these metadata to parent nodes using simple heuristics: (1) a parent node was annotated with a year if all of its descendants were annotated with that year, (2) a parent node was annotated with a particular country if all of its descendants were annotated with that country, (3) a parent node was annotated with the mean age of its (age-annotated) descendants. Nodes with descendants spanning multiple years and/or countries were rare. We also calculated a more nuanced time estimate for nodes using Chronumental⁵⁰. We used Taxonium⁴⁸, the UShER web interface⁴⁷, Nextstrain⁵¹ and Nextclade⁵² extensively in investigating individual branches of interest.

We defined “high G-to-A branches” as those with at least 10 mutations, of which $>90\%$ were transitions and $>25\%$ were specifically G-to-A mutations, with $>20\%$ C-to-T. Such a threshold appeared to yield very high specificity, as judged by the ability to detect marked changes in the rate of a rare event (molnupiravir treatment) over time. We also created simulated measures of sensitivity and specificity using the distribution of mutation types from Ruis et al. and Alteri et al. We performed these calculations for different branch lengths (n) from 10 to 20. In each case we performed 10,000 draws of n mutations from each of the naive and molnupiravir-associated mutational class distributions. We then assessed what proportion of these draws satisfied our criteria defined above. In the case of the molnupiravir-associated class distribution, this proportion represented the sensitivity. In the case of the typical-BA.1 distribution, this proportion represented $1 - \text{specificity}$. We obtained a sensitivity of 46% and a specificity of 98.9% for branch length 10, a sensitivity of 63% and a specificity of 98.6% for branch length 13, a sensitivity of 71% and a specificity of 98.6% for branch length 15, and a specificity of 64% and specificity of 99.8% for branch length 20.

To measure whether high G-to-A branches showed a statistically significant increase in mutation rate we used Chronumental's branch length estimates in time, and performed statistical testing with a two-sided t-test on nodes from 2022, looking only at nodes with at least 10 mutations.

To test whether age metadata differed according to the presence of the high G-to-A signature we took all USA nodes from 2022 that were above the minimum branch length (≥ 10) and divided them according to the presence or absence of the high G-to-A signature. We performed a two-sided t-test to test the significance of the effect seen. To verify that the effect was not substantially driven by the heuristic of taking the mean of descendant nodes, we repeated the analysis considering only branches with a single descendant, finding highly similar results.

Calculation of mutational spectra

To identify preferred nucleotide contexts for molnupiravir-based mutagenesis we calculated single-base substitution (SBS) spectra. For the high G-to-A branches, we extracted mutation paths from the UShER mutation-annotated tree. The context of each mutation was identified using the Wuhan-Hu-1 genome (accession NC_045512.2), incorporating mutations acquired earlier in the path. Mutation counts were rescaled by genomic content by dividing the number of mutations by the count of the starting triplet in the Wuhan-Hu-1 genome. MutTui (<https://github.com/chrisruis/MutTui>) was used to rescale and plot mutational spectra.

To calculate an SBS spectrum from the Alteri et al. dataset we used the mapped reads from BioProject PR-JNA854613, again taking sites which had ≥ 100 reads of which $\geq 5\%$ were distinct from the day 0 consensus. We rescaled mutation counts to mutational burdens by dividing each mutation count by the number of the starting triplet in the Wuhan-Hu-1 genome (accession NC_045512.2).

We performed a similar analysis for the Donovan-Banfield et al.²⁰. We used deep sequencing data from samples collected on day one (pre-treatment) and day five (post-treatment) from 65 patients treated with placebo and 58 patients treated with molnupiravir. For each patient, we used the consensus sequence of the day one sample as the reference sequence and identified mutations as variants in the day five sample away from the patient reference sequence in at least 5% of reads at genome sites with at least 100-fold coverage. The surrounding nucleotide context of each mutation was identified from the patient reference sequence.

To ensure that any spectrum differences between placebo and molnupiravir treatments are not due to previously observed differences in spectrum between SARS-CoV-2 variants^{19,21}, we compared the distribution of variants between the treatments (Extended Data 4). The distributions were highly similar.

We compared the contextual patterns within each transition mutation type, assessing the similarity of the values of the 16 possible tri-nucleotide context from the high G-to-A phylogenetic branches against those from the Alteri et al. dataset and, separately, those from the Donovan-Banfield et al. dataset and the Ruis et al. control spectrum. For each dataset combination, cosine similarities were calculated for each transition mutation class. We performed the same correlational analysis *within* the long branch data, comparing the G-to-A subset with the C-to-T subset, matching each G-to-A context to its reverse-complement in the C-to-T dataset.

Identifying highly divergent molnupiravir-derived sequences excluded from the mutation-annotated tree

Given that in the process of construction of the UShER mutation-annotated tree highly divergent sequences

can be excluded, we decided to perform a secondary analysis to identify divergent sequences with a molnupiravir signature. We used Nextclade⁵² for this task. We supplied a full dataset of full-length FASTA sequences, and every sequence that could be aligned with Nextclade was included. Nextclade places each sequence onto a sparse tree reference phylogenetic tree. Its outputs include a unlabelled private mutations column, which contains private mutations at a node with respect to the tree, excluding revertant mutations and mutations that are very common in other clades. We analysed this set of mutations for the presence of molnupiravir-like mutation-class distributions.

We selected sequences that had ≥ 20 mutations of which $\geq 20\%$ were G-to-A, $\geq 20\%$ were C-to-T and $\geq 90\%$ were transitions. Again these were heavily enriched for dates after the roll-out of molnupiravir. We placed identified sequences onto a downsampled global tree using *usher.bio* and visualised this tree using Nextstrain⁵¹.

To test whether the >100 mutations in the sequence shown in Fig. 4C had contexts more compatible with the molnupiravir spectrum we identify here or with typical BA.1 spectrum, we performed analysis with multinomial models. Here we aimed to ignore the signal from the mutations classes themselves (since these had been used to select the sequence as interesting) and to consider only the extra information added by the contexts in which transition mutations occurred. For each transition class (G-to-A, C-to-T, A-to-G, T-to-C) we created two multinomial models of trinucleotide context, one using the long-branch molnupiravir spectrum we define here, and one using the BA.1 spectrum from Ruis et al. In each case we multiplied by the number of times a trinucleotide context occurred in the genome to remove the previous normalisation against this parameter. We assessed the likelihood of observing the counts of contexts in the sequence of interest under both models and calculated a Bayes factor for each (G-to-A: 35017, C-to-T: 6068, A-to-G: 53, T-to-C: 1.22). These combine to give a Bayes factor of 1.4×10^4 .

Analysis of synonymous and non-synonymous mutations

We examined the types of mutations that made up these branches. We used BTE to determine whether each mutation observed was synonymous or not. Mutations were tallied by this status, grouped according to whether the branch was short (<10 mutations) or long (≥ 10 mutations), and whether it had a high G-to-A signature. We calculated the proportion of mutations that were non-synonymous in each case, calculated binomial confidence intervals for these proportions, and compared them using a two-sided test of equal proportions.

We plotted the distribution of mutations across the genome for high G-to-A branches, split according to whether the mutations were synonymous or not, and also plotting the distribution specifically for the most re-

current non-synonymous mutations, occurring in four or more high G-to-A branches. Kernel density estimates were made with a Gaussian kernel, and a bandwidth of 500 bp.

Processing and visualisation of cluster trees

The bulk trees presented in the supplement were plotted from the UShER tree using ggtree⁵³.

For the cluster of 20 individuals shown in Fig. 4A, we observed small imperfections in UShER's representation of the mutation-annotated tree within the cluster resulting from missing coverage at some positions. We therefore recalculated the tree that we display here. We took the 20 sequences in the cluster, and the three closest outgroup sequences, we aligned using Nextclade⁵², calculated a tree using iqtree⁵⁴ and reconstructed the mutation-annotated tree using TreeTime⁵⁵. We visualised the tree using FigTree⁵⁶.

Linkage analysis to treatment records

49 sequences with high G-to-A signatures from England, which fell into 35 clusters, were analysed by UKHSA. Sequences were linked to Blueteq treatment records³⁵ based on NHS number. Linkage could be established for all sequences. The analysis found that 11 of the 35 distinct clusters involved a molnupiravir-prescribed individual, giving a cluster hit-rate of 31%. Only sequences sampled after the treatment date were counted, with no upper time limit.

Limitations

There are some limitations of our work. Identifying a particular branch as possessing a molnupiravir-like signature is a probabilistic rather than absolute judgement: where molnupiravir creates just a handful of mutations (which trial data suggests is often the case), branch lengths will be too small to assign the cause of the mutations with confidence. We therefore limited our analyses here to long branches. This approach may also fail to detect branches which feature a substantial number of molnupiravir-induced mutations alongside a considerable number of mutations from other causes (which might occur in chronic infections). Our approach to identifying molnupiravir-associated sequences used simple thresholding on the proportion of mutations on a branch with different classes of mutation. The simplicity of this approach, which does not make detection probability a function of branch length, enabled us to perform analyses such as looking at the distribution of branch length in different conditions, but future analyses which increase sensitivity with more nuanced statistical approaches (with which we did experiment, finding the simple method preferable in this first case for the flexibility it offered), as well as considering the contextual mutation spectrum itself as a signal for detection, will both be valuable in future work.

We discovered drastically different rates of molnupiravir-associated sequences by country and suggest that this

reflects in part whether, and how, molnupiravir is used in different geographical regions; however, there will also be contributions from the rate at which genomes are sequenced in settings where molnupiravir is used. For example, if molnupiravir is used primarily in aged-care facilities and viruses in these facilities are significantly more likely to be sequenced than those in the general community this will elevate the ascertainment rate of such sequences. Furthermore, it is likely that some included sequences were specifically analysed as part of specific studies because the samples demonstrated continued test positivity after molnupiravir treatment. Such effects are likely to differ based on sequencing priorities in different locations. We identified sequence clusters descending from high G-to-A nodes. In a number of cases, detailed and distinctive metadata show that a particular cluster is made up of sequences from different patients, suggesting transmission of molnupiravir-induced mutations; however in the absence of such data, clusters are also compatible with representing multiple samples taken from a single individual.

Our analysis here looked at consensus sequences, which means that for a mutation to be detected it must reach a high proportion of the population in the host. Analyses that look at deep sequencing data, and also mixed base-calls in consensus sequences, will be valuable.

ACKNOWLEDGEMENTS

We gratefully acknowledge all data contributors, i.e., the Authors and their Originating laboratories responsible for obtaining the specimens, and their Submitting laboratories for generating the genetic sequence and metadata and sharing via the GISAID Initiative, on which this research is based. We are also very grateful to everyone who has contributed to the generation of the genomes that have been deposited in the INSDC databases, on which this research is also based. We thank Angie Hinrichs and colleagues for access to an UShER mutation-annotated tree built with all available genomic data. We would also like to acknowledge NHS England for providing the Blueteq data on treatment records. We would like to acknowledge the UKHSA COVID-19 Therapeutics Programme Team past and present, in particular Jordan Charlesworth, Angie Lackenby, Alicia Demirjian, Meera Chand and Colin Brown. We thank Jesse Bloom, Michael Lin, Richard Nether, Kelley Harris and Florence Débarre for useful discussions. This preprint uses a LaTeX template from Stephen Royle and Ricardo Henriques. The opinions are those of the authors and not necessarily those of UKHSA.

AUTHOR CONTRIBUTIONS

RH identified initial branches, and their likely connection to molnupiravir. TS performed analyses of mutation-annotated tree and global metadata. CR led mutational spectra analyses. ID-B created bioinformatic pipelines for AGILE trial data. TPP functionally curated mutations identified in long branches. HH and AL performed linkage analyses. All authors participated in manuscript writing.

COMPETING INTERESTS

The authors declare no competing interests.

CORRESPONDENCE

Correspondence and requests for materials can be addressed to Theo Sanderson (theo.sanderson@crick.ac.uk).

DATA AVAILABILITY

No new primary data was generated for this study. We used data from consensus sequences available through GISAID and the INSDC^{24,25}, from the AGILE clinical trial²⁰, where genomic data were obtained from BioProject PRJNA854613 at the SRA, and from Alteri et al¹⁸ from BioProject ERP142142. The AGILE investigators were not involved in the analysis and preparation of this manuscript.

Linkage analysis was performed within UKHSA. Section 251 of the National Health Service Act 2006 permits UKHSA use of patient-level data for specific projects.

The findings of this study are based on metadata associated with 15,572,413 sequences available on GISAID up to June 2023, and accessible at [10.55876/gis8.230110wz](https://gisaid.org/seqs/10.55876/gis8.230110wz), and [10.55876/gis8.230110db](https://gisaid.org/seqs/10.55876/gis8.230110db), [10.55876/gis8.230622mw](https://gisaid.org/seqs/10.55876/gis8.230622mw) (see also, Supplemental Tables). The findings of this study are also based on 7,104,124 sequences from INSDC – authors, metadata, and sequences are available [here](#). Data present in both databases are deduplicated during the construction of the mutation-annotated tree on the basis of sequence, name, and metadata. We standardised to GISAID sequence names and accessions for sequences present in both databases.

A version of our analysis using only the INSDC subset of the tree, with INSDC naming conventions, is available at https://github.com/theosanderson/molnupiravir/tree/main/open_data_version.

CODE AVAILABILITY

Our GitHub repository is located at <https://github.com/theosanderson/molnupiravir>. It is archived on Zenodo: [10.5281/zenodo.8101003](https://doi.org/10.5281/zenodo.8101003)

FUNDING

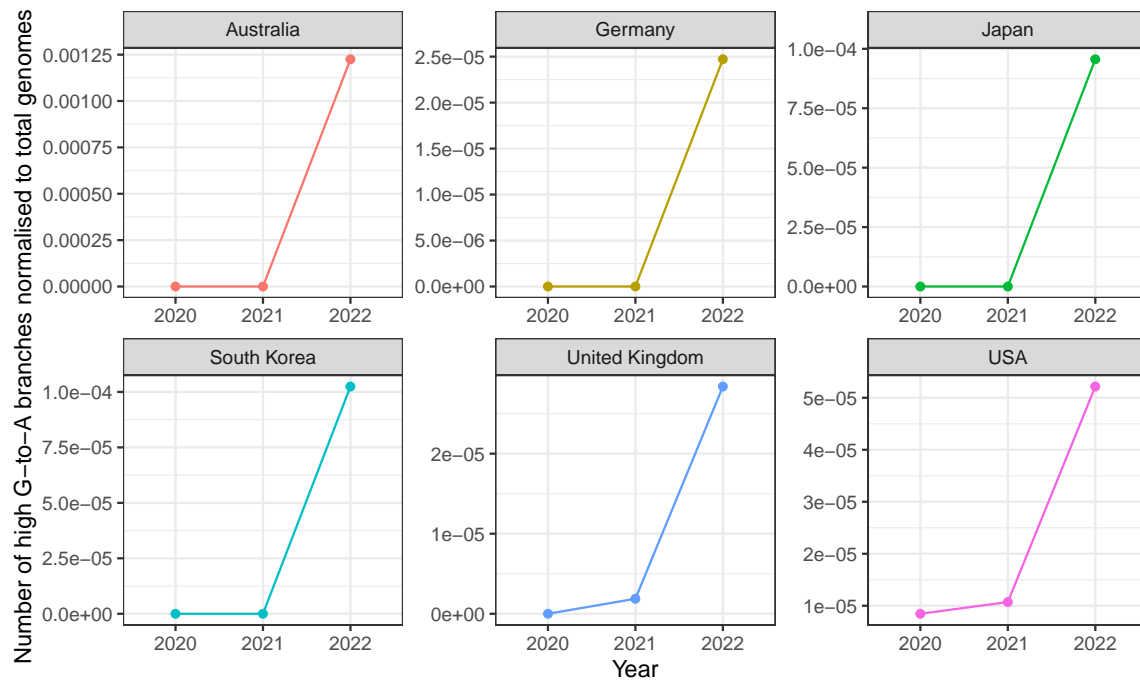
TS was supported by the Wellcome Trust (210918/Z/18/Z) and the Francis Crick Institute which receives its core funding from Cancer Research UK (FC001043), the UK Medical Research Council (FC001043), and the Wellcome Trust (FC001043). This research was funded in whole, or in part, by the Wellcome Trust [210918/Z/18/Z, FC001043]. For the purpose of Open Access, the authors have applied a CC-BY public copyright licence to any Author Accepted Manuscript resulting from this preprint.

ID-B is supported by PhD funding from the National Institute for Health and Care Research (NIHR) Health Protection Research Unit (HPRU) in Emerging and Zoonotic Infections at University of Liverpool in partnership with Public Health England (PHE) (now UKHSA), in collaboration with Liverpool School of Tropical Medicine and the University of Oxford (award 200907). The views expressed are those of the authors and not necessarily those of the Department of Health and Social Care or NIHR. Neither the funders or trial sponsor were involved in the study design, data collection, analysis, interpretation, nor the preparation of the manuscript.

TPP was funded by the G2P-UK National Virology Consortium funded by the MRC (MR/W005611/1).

CR was supported by a Fondation Botnar Research Award (Programme grant 6063), the UK Cystic Fibrosis Trust (Innovation Hub Award 001) and funding from the Oxford Martin School.

Extended data

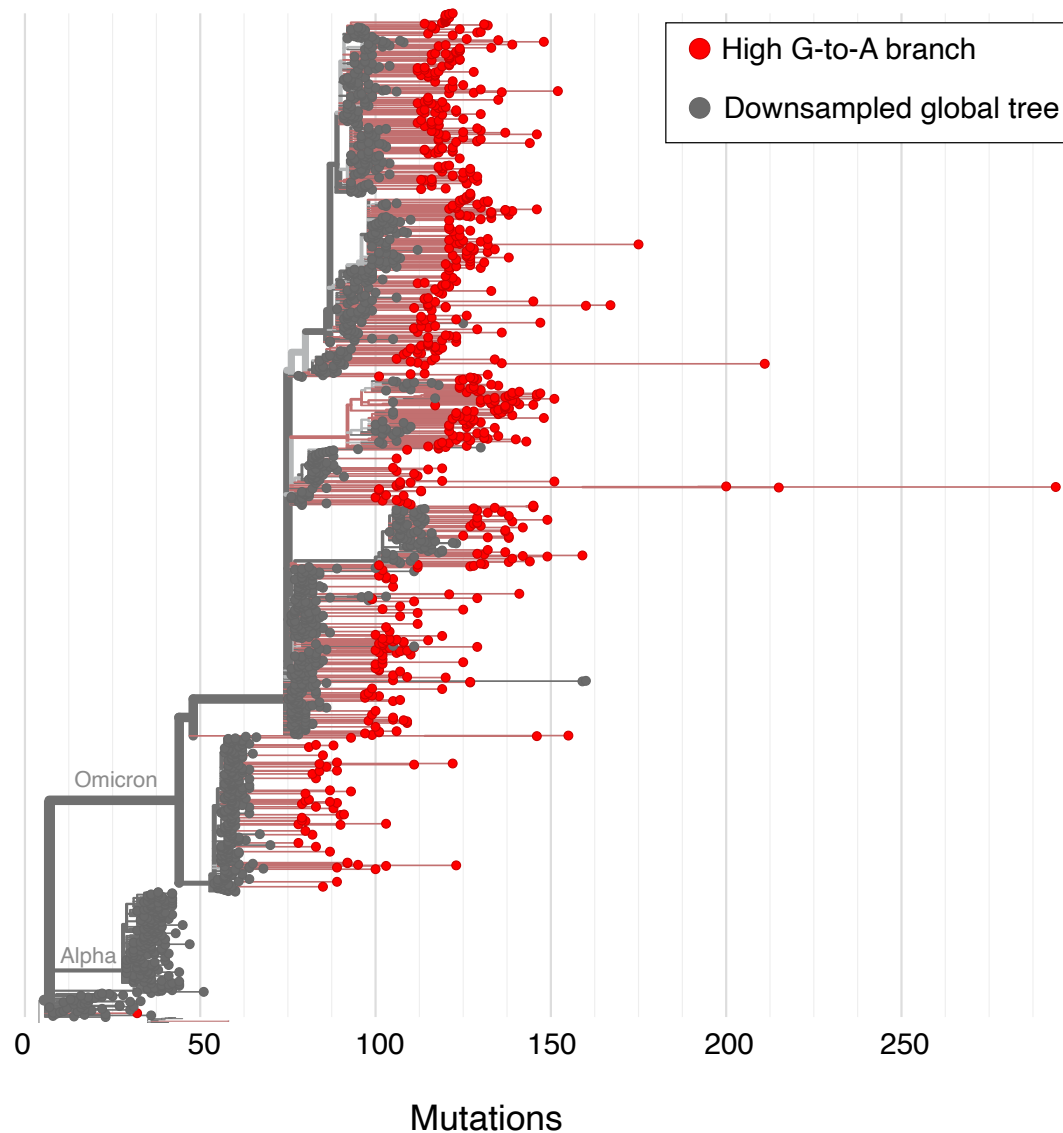


Extended Data 1. Timeline of number of high G-to-A branches, normalised for sequencing volumes, in 6 countries

The y-axis represents number of high G-to-A branches, divided by total sequencing volume for the year. This analysis demonstrates that the effects seen in raw numbers in Fig. 2D cannot be explained by changes in sequencing volume.

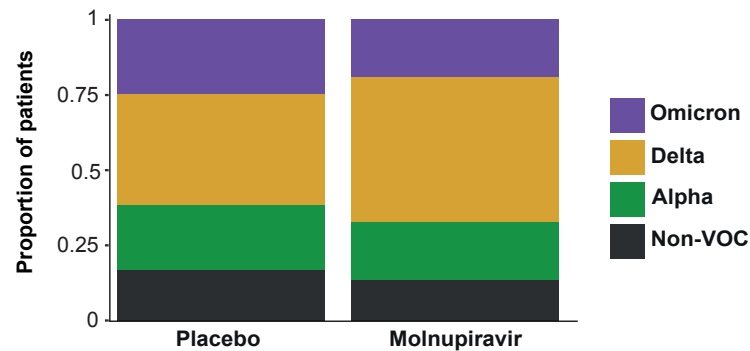
Country	High G-to-A branches in 2022	Total genomes in 2022
Australia	149	121,602
USA	106	2,031,795
United Kingdom	35	1,232,969
Japan	35	366,060
Russia	17	41,416
Germany	13	525,967
Italy	13	70,555
Israel	12	108,770
Slovakia	11	26,461
Denmark	10	332,006
Thailand	9	24,338
Austria	8	46,962
Spain	7	95,635
New Zealand	7	25,170
South Korea	6	58,567
Turkey	6	20,754
France	4	328,527
Czech Republic	4	32,124
Ireland	3	48,704
Indonesia	3	34,499
Luxembourg	3	30,715
India	2	121,841
Belgium	2	84,600
Philippines	2	12,830
Canada	1	217,040
Sweden	1	88,418
Poland	1	44,014
Mexico	1	35,857
Slovenia	1	31,221
Norway	1	30,796
South Africa	1	15,502
Latvia	1	14,039
Hong Kong	1	10,969
Brazil	0	98,346
Netherlands	0	64,614
Switzerland	0	49,062
Peru	0	30,772
Malaysia	0	27,113
Croatia	0	22,786
Chile	0	20,229
Portugal	0	19,483
Finland	0	18,518
Singapore	0	17,353
Greece	0	14,293
Colombia	0	12,302
China	0	11,425
Lithuania	0	10,059

Extended Data 2. Number of high G-to-A branches from 2022 against total number of genomes from 2022 by country.
Only countries with >10,000 genomes are included.



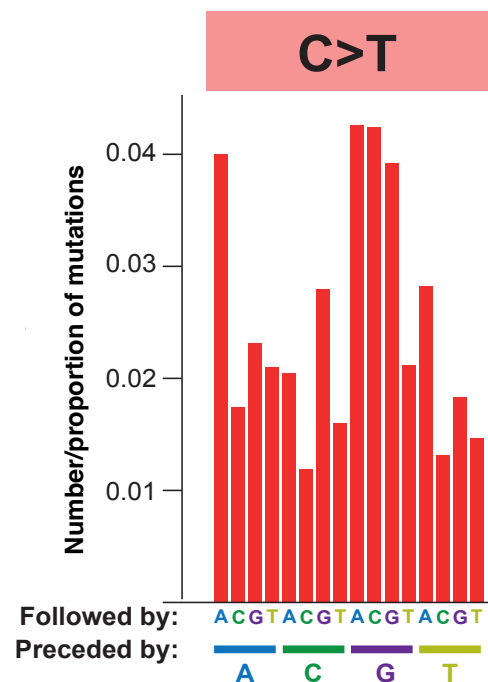
Extended Data 3. High G-to-A sequences with more than 20 private mutations identified from a Nextclade alignment of all available SARS-CoV-2 sequences

Nextclade was used to align sequences and identify private mutations. High G-to-A branches were identified on the basis of unlabelled private mutations. Usher.bio was then used to create a tree with high G-to-A branches highlighted on a downsampled global tree, with visualisation performed with Nextstrain.



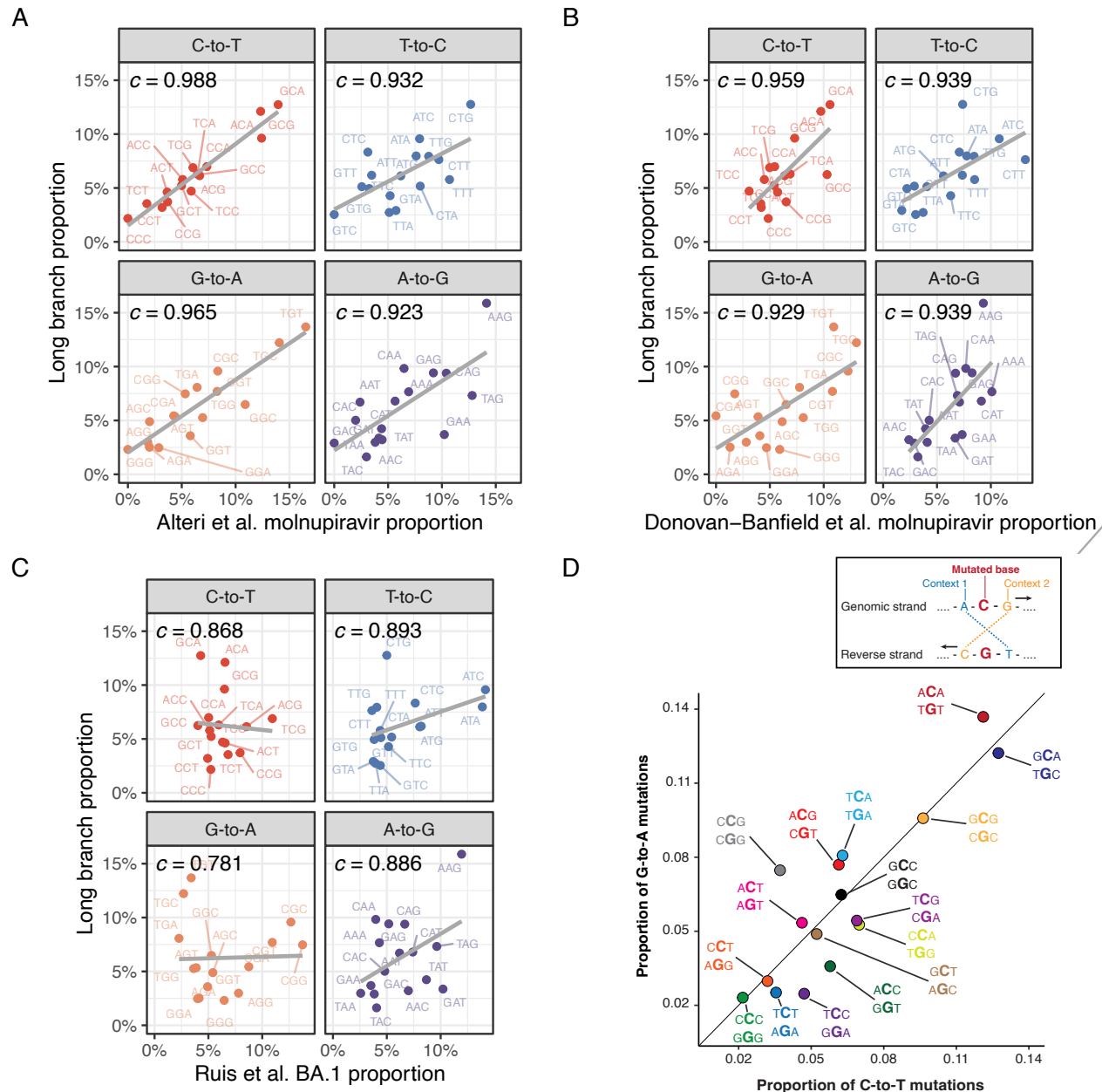
Extended Data 4. Distribution of major SARS-CoV-2 variants between placebo and molnupiravir treatments in the AGILE trial dataset.

The proportion of patients infected with each variant is shown. The proportions are similar suggesting that differences between placebo and molnupiravir spectra will not be influenced by previously observed spectrum differences between variants (Ruis et al., Bloom et al.). VOC = variant of concern.



Extended Data 5. Context locations within the mutational spectrum.

The RNA mutational spectrum contains 12 mutation types, for example C-to-T, shown here. The spectrum also captures the nucleotides surrounding each mutation. There are four potential upstream nucleotides and four potential downstream nucleotides. This figure shows the location of each of the 16 contexts within an example mutation type. For example, the leftmost bar represents C-to-T mutations in the ACA context while the second leftmost bar represents C-to-T mutations in the ACC context. The spectrum represented is from AGILE trial data on molnupiravir.



Extended Data 6. Mutation spectrum analysis supports a molnupiravir origin for high G-to-A nodes

(A) Strong correlation for contexts in all transition mutation classes between Alteri et al. molnupiravir-treated patients and high G-to-A long branches. (B) Similar analysis, with clear correlation between Donovan-Banfield et al. dataset of molnupiravir treated individuals to long high G-to-A branches. (C) Little correlation seen between contexts in typical SARS-CoV-2 evolution (Ruis et al.) and high G-to-A branches. (D) In data from long branches, context proportions for G-to-A mutations correlate with context proportions for C-to-T mutations, indicating a common mutational process. Points are labelled with G-to-A context, then C-to-T context.